

**[PRE-PRINT]**

**Improving HF Radar Surface Current Measurements  
with Measured Antenna Beam Patterns**

ACCEPTED FOR PUBLICATION AS ARTICLE IN  
JOURNAL OF ATMOSPHERIC AND OCEANIC TECHNOLOGY  
AS OF JANUARY 14, 2003 AND WILL BE PUBLISHED FALL 2003

Online Preprint Available:

<http://marine.rutgers.edu/cool/coolresults/papers/papers.html>

**Authors:**

**[Dr. Joshua Kohut](#)**

**Institute of Marine and Coastal Sciences  
Rutgers, The State University of New Jersey  
New Brunswick, New Jersey**

**and**

**[Dr. Scott Glenn](#)**

**Institute of Marine and Coastal Sciences  
Rutgers, The State University of New Jersey  
New Brunswick, New Jersey**

## **ABSTRACT**

A High Frequency (HF) radar system is deployed on the New Jersey continental shelf as part of a coastal ocean observatory. The system includes two remote transmit/receive sites in Brant Beach and Brigantine, New Jersey and a central processing site in Tuckerton, New Jersey. The system uses radio waves scattered off the ocean to measure the radial velocity, range, and bearing of the scattering surface. Calculation of the bearing for HF radar systems depends on the actual beam pattern of the receive antennas. A series of antenna beam pattern measurements conducted on the New Jersey system show that these patterns are often distorted when an antenna is deployed in the field. Tests indicate that the local environment, not system hardware, causes the most significant distortion of the pattern from the theoretical shape. Correlation with an in situ Acoustic Current Doppler Profiler (ADCP) indicates that the beam pattern distortion can bias the bearing estimate. It is shown that this bias can be removed if the measured beam patterns are used to estimate the bearing.

## 1. Introduction

High Frequency (HF) radar systems have matured to the point where they are now integral components of coastal ocean observation networks and prediction systems (Glenn et al. 2000b; Paduan et al. 1999). HF radar uses scattered radio waves to measure surface currents, wave parameters and surface wind fields (Paduan and Graber 1997; Wyatt 1997; Graber and Heron 1997; Fernandez et al. 1997). Surface currents, the most common product of HF radar systems, are used for real-time applications (Kohut et al. 1999), data assimilation and model validation (Breivik and Sætra 2001; Oke et al. 2000; Shulman et al. 2000), and dynamical studies (Shay et al. 1995, Kosro et al. 1997; Paduan and Cook 1997). This expanding HF radar user community necessitates a better understanding of system operation and accuracy.

There is a thirty-year history of validation studies using *in situ* observations to ground truth HF radar data. Early studies compared total vector current data measured with HF radar and *in situ* current meters, including Acoustic Doppler Current Profilers (ADCPs) and drifters, reporting RMS differences ranging from 9 to 27 cm/s (for a review see Chapman and Graber 1997). All agree that physical differences between the types of measurements must be considered when validating HF radar data with *in situ* instruments. These differences can be separated into three categories, velocity gradients (vertical and horizontal), time averaging, and geometric error associated with total vector combination.

A HF radar system operating at a typical frequency of 25 MHz uses the scattered signal off of a 6 m long surface gravity wave to infer near surface current velocities. These current measurements are vertically averaged over the depth felt by the wave. Assuming a linear velocity profile, Stewart and Joy (1974) estimate that for a 6 m long ocean wave, this depth is about 1 m. At this frequency, any velocity shear between the upper 1m of the water column and

the depth of the *in situ* measurement will affect the RMS difference. Graber et al. (1997) demonstrate that the contribution of specific upper ocean processes including Ekman fluxes can lead to differences between remote HF radar and *in situ* current measurements. Additional horizontal differences occur since HF radars are calculating currents based on a return signal that, for a typical 25 MHz system, is averaged over a patch of the ocean surface that can be as large as 3 km<sup>2</sup>, while typical *in situ* current meters measure at a single point. Any surface inhomogeneity like fronts or small eddies will contribute to the observed RMS difference.

The second contribution to the difference is the time sampling of the two instruments. A typical 25 MHz system averages the continuous backscattered data into hourly bins. Often *in situ* measurements are burst sampled because of battery power and data storage requirements. High frequency oscillations such as internal waves could contaminate a short burst in the *in situ* measurement and be averaged over in the HF radar data.

The third possible contribution to the RMS difference between HF radar and *in situ* measurements is related to the geometric combination of radial velocity vectors. Since HF radar systems use Doppler theory to extract surface current information, standard backscatter systems can only resolve the radial current component directed toward or away from the antenna site. At least two spatially separated sites are necessary to calculate the total vector currents for the ocean surface. An example of a radial component velocity map is shown for two coastal sites in Figure 1. When estimating the total current vector from radial components, the further the two radials are from orthogonality, the larger the potential error in the total vector. This is described by Chapman et al. (1997) as the Geometric Dilution Of Precision (GDOP). By using the independent radial velocity measurements from the two remote sites, this study eliminates this error seen exclusively in the total vector calculations.

More recently, the role of receive antenna patterns on system accuracy has been the focus of HF radar validation. Barrick and Lipa (1986) used an antenna mounted on an offshore oilrig to illustrate that near-field interference can cause significant distortion from ideal patterns. Their study defines this near-field as a circle around the antenna with a radius equal to one wavelength of the broadcast signal. Through simulations, they show that typical pattern distortion can introduce an angular bias as large as 35 degrees if they are not taken into account. Comparisons of radial velocity vectors calculated directly between two HF radar sites located on opposite shores of Monterey Bay, California have also shown an angular bias between the baseline and the best correlation (Fernandez and Paduan 1996). It is suggested that this bias could be caused by distorted antenna patterns. More recently, Paduan et al. (2001) show that the HF radar correlation with observed currents from an ADCP improves if pattern distortion is taken into account. Kohut et al. (2000) also show the importance of pattern distortion and go on to identify possible sources of this distortion including hardware and the local environment. The HF radar validation results presented here will investigate several sources of antenna pattern distortion as measured in the field, and quantify how this distortion impacts system accuracy. Section 2 briefly describes those features of the operation of HF radar systems relevant to the ensuing discussion. Section 3 outlines the specific instrumentation and methods used in this study. Section 4 discusses the source of antenna pattern distortion and the impact of this distortion on system accuracy, and section 5 presents some concluding remarks.

## **2. Background**

HF radar systems use the return signal scattered off the ocean surface to measure the range, bearing and radial velocity of the scattering surface towards or away from the antenna.

The radial velocity is determined using Bragg peaks in the spectra of the backscattered signal (Barrick 1972; Barrick et al. 1977; Lipa and Barrick 1986). Crombie (1955) first recognized that these peaks were the result of an amplification of a transmitted signal by surface gravity waves with a wavelength equal to half that of the transmitted signal. The range of the scattering surface is measured using either a time delay or a frequency modulation technique. The methods used to measure the range and radial velocity of the scattering surface are similar for all HF radar systems (Paduan and Graber 1997). Bearing determination, however, differentiates HF radar systems into two major types, Beam Forming (BF) and Direction Finding (DF). Both types illuminate the ocean surface over all angles with a transmitted signal. The difference arises in the reception and interpretation of the backscattered signal. A BF system uses a linear array of vertical elements to steer the receive antenna look angle to different bearings. The bearing of the measured return signal is the look angle of the receive antenna. Some systems mechanically rotate the transmit and receive antenna array (Furukawa and Heron 1996) and others use the relative phases of the antenna elements and their antenna beam patterns to move the receive antenna look angle across the ocean surface. The angular width of the look angle depends on the length of the linear array. A typical 25 MHz system requires an 80 m length to resolve 5 degree bins. In contrast, a DF system measures the return signal continuously over all angles. The beam patterns of independent antenna elements are used to determine the direction of the incoming signals. The angular resolution, set in the processing, is typically 5 degrees. For a description of the mechanics and operation of these two HF radar systems, the reader is referred to Teague et al. (1997) and Barrick and Lipa (1996).

Coastal Ocean Dynamics Applications Radar (CODAR), a DF system, uses a three element receive antenna mounted on a single post. These elements include two directionally

dependent cross-loops and a single omnidirectional monopole (Lipa and Barrick, 1983; Barrick and Lipa, 1996). Since the monopole is omnidirectional, the antenna pattern is a circle of constant radius around the antenna post. Since the absolute patterns of each element cannot be measured, all the patterns discussed in this paper are those of the loops normalized by the monopole (Figure 2). This normalized pattern can be measured in the field and used in the current processing algorithms. The theoretical (ideal) pattern has a peak in loop 1 that coincides with the null of loop 2 and vice versa. Using a frequency modulation technique (Teague et al. 1997), the continuous data measured by each antenna is separated into distinct range cells. One range cell of a typical radial field is highlighted in Figure 1. The Bragg peaks are used to calculate all the radial velocities measured in the range cell. The bearing of each radial velocity is then determined using the frequency spectra from each receive antenna element. Since its inception, the CODAR system has used several different algorithms to determine the bearing of a given radial velocity, including a closed form solution and a least squares fit to the incoming data (Lipa and Barrick 1983; Barrick and Lipa 1986). More recently, a much more robust Multiple Signal Classification (MUSIC) algorithm enables the CODAR configuration to resolve more complicated flow fields, including conditions when the same radial velocity comes from two different directions. MUSIC was first developed by Schmidt (1986) to locate radio signal sources from aircraft. Barrick and Lipa (1999) have modified MUSIC for the specific task of extracting the bearing of a given signal measured by  $N$  isolated antenna elements. The algorithm has been evaluated and fine-tuned using simulations to recreate known radial velocity fields (Barrick and Lipa 1997 and Laws et al. 2001). In its present form, MUSIC can use the shape of either the ideal or measured normalized beam pattern to determine the bearing of a signal scattered off the ocean surface.

The measured antenna pattern differs from the ideal due to distortion caused by coupling with any object other than air within the near-field (about 1 broadcast wavelength). The most significant coupling will occur with objects larger than  $1/4$  wavelength, especially vertical conductors since the HF radar signals are vertically polarized to enable propagation over the ocean surface. The vertical antenna elements in any HF radar system are more susceptible to beam pattern distortion. For the CODAR-type system the cross-loops are less sensitive since any additional current induced on one side of the loop is approximately balanced by an opposing current induced on the opposite side. Rather than normalizing one cross-loop by the other, measured beam patterns for each loop will be normalized by the monopole (as in Figure 2) to maximize our ability to identify distortion. Under ideal conditions, the geometry of a CODAR-type system with a single monopole and two cross-loop elements is such that all current carrying paths of the elements are orthogonal to each other. This orthogonality inhibits any one element from interacting with the other two. When the antenna is mounted in the field, either the local environment or system hardware could induce coupling and change this ideal condition. If the geometry breaks down, the antenna elements interact, causing the normalized ideal pattern to distort. This study will examine the effect of system hardware and the local environment on antenna patterns, and compare ocean currents estimated with both the ideal and measured patterns with *in situ* surface current measurements.

### **3. Methods**

#### *a) HF Radar Setup*

The 25 MHz CODAR system used here includes two remote antenna sites separated by 26 km in Brant Beach and Brigantine, New Jersey (Figure 1). The first deployment of this

system ran from May 1998 to August 1998. The success of this first summer test prompted a second continuous deployment that began nine months later in May of 1999 and is continuing to sample in real-time, surviving tropical storm Floyd (Kohut 2002) and many nor'easters. Since the remote sites can only resolve the component of the velocity moving toward or away from the antennas, radial current maps are generated at each site. Each field has a range resolution of 1.5 km and an angular resolution of 5 degrees. The radial velocities are based on hourly averaged backscatter data. The fields are center averaged at the top of the hour. This study uses radial velocities collected between October 16, 1999 and January 24, 2000. By using the radial velocity components from each site, the contribution of GDOP is eliminated from the investigation.

The normalized antenna patterns were measured using a transponder that modifies and re-radiates the transmitted signal (Barrick and Lipa 1986; Barrick and Lipa 1996). The small battery operated transponder is mounted on the deck of a boat that tracks along a semi-circle around the receive antenna, maintaining a constant speed and radius. For this particular study, the boat maintained a range of 1 km and a speed of 5 knots. At the remote site, raw time series data were measured by each receive element. The time series were combined with the boat's GPS data to determine how the transponder signal varied with angle for each antenna element.

Table 1 summarizes the pattern runs completed at the two CODAR sites. Each pattern run is the average of two boat transects, one circling north to south and the other circling south to north. The distortion for each run is calculated by subtracting the measured pattern from the ideal pattern. Since the pattern amplitudes are continually adjusted with sea echo (Lipa and Barrick 1983), the ideal pattern is taken as the best-fit cosine through the measured pattern (Figure 2). The sites in Table 1 are labeled according to the characteristics of the near field. Both sites,

operating at 25.41 MHz and 24.70 MHz, have a near-field with a radius of about 12 m. The antenna setup in Brant Beach is mounted on a sand dune close to the surf zone where there are no buildings or any other known interference within several wavelengths of the antenna. This site has a clear near-field and will be referred to as the clear site. In Brigantine, the antenna is mounted on a sand dune within one wavelength of a four-story condominium. The presence of this large building clutters the antenna's near-field, so the Brigantine site will be referred to as the cluttered site. The ground plane length referred to in Table 1 is the length of the four horizontal fiberglass whips that make up the ground plane of the monopole element. During normal operation, antenna A and receiver A are the receive antenna and receiver setup at the clear site, and antenna B and receiver B are setup in the cluttered site.

The bearing of each radial velocity in a given range cell was calculated once with the ideal pattern and twice with the measured pattern, both with and without outlier elimination, angular interpolation, and smoothing. Outliers were identified using the median of the vectors that fall within 20 degrees of the data point. If the data value is more than 25 cm/s from the median value, it is eliminated from the radial field. The interpolation algorithm then uses a Gaussian window with a half power width of 20 degrees to smooth and interpolate the data. Radial velocities that are more than 10 degrees from the interpolated value are weighted significantly less than data within 10 degrees of the interpolated radial velocity (Barrick and Lipa 1996). This algorithm is used exclusively on the measured pattern current estimates.

#### *b) ADCP Setup*

A single bottom-mounted ADCP was deployed at the Longterm Ecosystem Observatory (LEO-15) from September 21, 1999 to February 29, 2000 (Grassle et al. 1998; Glenn et al.

2000a; Schofield et al. 2001). Real time data was sent from the seafloor node through a fiber optic cable to a computer on shore. The location of this ADCP is shown in Figure 1. The ADCP operated at 1200 kHz with a bin resolution of one meter. The ADCP continuously sampled in mode-1 at a sample rate of 400 pings per one minute ensemble. Since the ADCP was continuously sampled, the potential difference due to burst sampling was eliminated from the dataset. These data were hourly averaged centered at the top of the hour to exactly match the sampling of the CODAR systems. The shallowest bin without sidelobe interference was used in the comparisons. This bin was determined for each data point using the ADCP pressure record by maintaining a depth of about 2.5 meters below the surface. The resulting ADCP comparison is then as close to the surface as possible throughout the entire record. The north/south and east/west components of the velocity measured in the surface bin were rotated into a radial/cross-radial coordinate system for each site. The radial component of the ADCP data was compared directly to the radial CODAR data, eliminating the error due to GDOP.

#### **4. Results and Discussion**

##### *a) Antenna pattern distortions*

###### 1) Ground plane

The ground plane of the monopole is made up of four horizontal fiberglass whips at the base of the antenna box. These four orthogonal whips are oriented in the alongshore and cross-shore directions. For the remainder of the discussion, all patterns refer to the patterns of loops 1 and 2 normalized by the monopole. Pattern measurement runs tested two whip lengths, 1.2 m and 2.4 m, in each environment. Runs 3 and 4, completed approximately thirty minutes apart, measured the pattern of antenna A with the two different ground planes in the clear environment.

The patterns show that the 2.4 m ground plane causes a much larger distortion than the shorter ground plane (Figure 3a and 3b). The patterns indicate a stronger coupling between the ground plane and the two loops with the longer ground plane. At an operating frequency of 25 MHz, 2.4 m is a quarter wavelength. This quarter wave ground plane is resonant and therefore very efficient. The stronger currents within the ground plane induce strong signals on the two loops resulting in significant pattern distortion. When the whips are reduced to 1.2 m, the efficiency of the ground plane is reduced and the magnitude of the coupling diminishes. The influence of element interaction on antenna pattern distortion has been studied theoretically using an exact industry standard Numerical Electromagnetics Code (NEC) ideally suited for HF (Burke 1992). These studies have shown that the resonant ground plane will amplify the coupling between antenna elements. The observations measured in the clear environment support the theoretical results of the NEC.

The distortion of the pattern measured with the resonant (2.4 m) ground plane is relatively larger near the endpoints (Figure 3a). Since these patterns are measured using a transponder mounted on a boat, the pattern endpoints correspond to the coast on either side of the antenna. As the transponder gets close to the coast, the signal must travel over more of the beach to get to the antenna. When a signal travels over a less conductive surface, like sand, the signal strength quickly drops off. The increased distortion seen near the edges of the pattern is correlated with this weaker transponder signal. Theory suggests that pattern distortions caused by coupling between the individual elements will be relatively larger for angles with relatively weaker signals (Burke 1992). The larger distortion at the endpoints of the pattern further supports the antenna element interaction seen with the resonant ground plane.

The sensitivity of the antenna pattern to the length of the ground plane was also tested in the cluttered environment. Runs 1 and 2 measured the pattern of antenna B with the resonant (2.4m) and non-resonant (1.2m) ground planes. The pattern measured with the resonant ground plane has significant distortion over all angles (Figure 4a). The pattern with the non-resonant ground plane has less distortion, especially near the edges (Figure 4b). While changing the ground plane improves the pattern near the edges, the non-resonant pattern remains more distorted than the pattern measured in the clear site with the same setup. The remainder of this section will test and discuss the contribution of several possible sources responsible for this difference, including system hardware and the local environment.

## 2) Receiver

The receiver is the interface between the computer, the receive antenna and the transmitter. It houses the hardware components responsible for generating the transmitted signal and receiving the backscattered signal. The three coaxial cables from the antenna elements are attached to the back of the chassis. During these tests beam patterns using receivers A and B were measured in the clear environment. The patterns measured with the different receivers in the same environment show no significant difference (Figure 3b and 3d). Both patterns show relatively small distortion over all angles. The similarity between these two patterns indicates that the receiver does not account for the difference seen in the patterns measured at the clear and cluttered environments with the non-resonant ground plane.

## 3) Cables

The receive cables run from the receiver to the antenna elements. Electrical currents can build up along the cables and disrupt the ideal geometry discussed previously. If these currents exist, then the location of the cables with respect to the antenna could change the measured pattern. During normal operation these currents are inhibited by a tight loop in the cables near the base of the antenna. To test the effectiveness of this loop, the same system setup was measured with two different cable locations. During run 2, the cables were run as they would be during normal continuous operation. For run 12, the cables were moved closer to the ocean, maintaining the tight loop near the base of the antenna. A comparison between these runs shows that there is no significant difference between the patterns (Figures 4b and 4c). Based on these results, we conclude that the cable loop is an effective way to reduce electrical currents along the receive cables that can lead to pattern distortion.

#### 4) Receive antenna

The receive antenna consists of three independent antenna elements. Antennas A and B were switched so that the normalized patterns of both antennas could be measured in each environment. Runs 4 and 6 illustrate the difference between the patterns of antenna A and antenna B in the clear environment. The patterns of the two antennas in the clear environment are not significantly different (Figures 3b and 3c). There are some small differences, however they are much smaller than those seen in the patterns of the two antennas in different environments. Patterns for the two antennas were also measured in the cluttered environment (Figure 4b and 4d). Again they are very similar and both show significant distortion across much of the pattern. These results indicate that the antenna hardware does not account for the difference in the patterns measured at each site with the non-resonant ground plane.

### 5) Local environment

Patterns measured with the same hardware in the clear and cluttered environments were used to determine the impact of the local environment on antenna pattern distortion. Antenna B was measured in the clear and cluttered environments. The pattern in the cluttered environment is significantly distorted from the theoretical ideal pattern (Figure 4b). When this antenna is moved to the clear site these distortions are significantly reduced (Figure 3c). The results for antenna A show a similar trend in that the patterns measured at the cluttered site are significantly more distorted than those measured at the clear site (Figures 3b and 4d). Recently the cluttered site was moved 500 m to the southwest to a more stable beach location. The new location offers a more open near-field on a dune similar in composition to the setup at the clear site. After antenna B was moved the patterns were re-measured. The pattern measured at the new location is much closer to ideal than at the previous location (Figure 4e). These observations clearly indicate that interference within the antenna's near-field significantly influences pattern distortion. If either antenna A or B is set up in a clear environment, the patterns are much closer to ideal than if the same antenna is measured in a cluttered environment.

### 6) Time dependence

The time dependence of the measured patterns is very important to document since the patterns can be used to improve HF radar measurements. The time scale of the pattern changes will dictate the frequency of the measurement necessary to maintain accurate systems. The time dependencies of these patterns were determined by comparing like runs measured at different times. Both runs 4 and 5 measured the same system hardware in the clear environment 11

months apart. The measurements indicate that while the amplitude of the pattern changed over time, the angular dependence of the pattern did not (Figure 2 and 5a). These patterns are normalized by the omnidirectional monopole. If the strength of the monopole decreases, the amplitude of the normalized pattern will increase. Since the change in the pattern is felt equally over all angles, the difference in the normalized pattern can only be attributed to a weaker monopole. During the hardware changes for runs 6 and 7, the cable connecting the receiver to the monopole was disconnected and reconnected. The same hardware was then measured again in run 8. After the cable was reconnected, the pattern amplitude returned to the same order seen 11 months before (Figure 2 and 5b). Again the directional dependence of the pattern did not change. The tighter cable connection strengthened the monopole and decreased the amplitude of the normalized pattern. This indicates that the only change seen in the antenna pattern over the 11 month period is the strength of the monopole.

Similar tests were completed in the cluttered environment. These runs measured the same system setup 13 months apart. Again the amplitude, not the directionality, of the pattern was affected. The amplitude measured in October 1999 is on the order of 0.80. The amplitude of the same system setup measured 13 months later increased to about 1.50. After several hardware changes, the monopole connection was strengthened and the pattern amplitude returned to 0.65, the same order as that measured 13 months before. Through all of these runs the directional dependence of the patterns remained the same. Since the pattern amplitudes are adjusted with measured sea echo (Lipa and Barrick 1983), it is only required that the directional dependence of the pattern be maintained. The results from both sites indicate that the directionality of the normalized pattern measured in either environment did not significantly

change over annual time scales. Based on these conclusions, annual antenna pattern runs appear to be sufficient to maintain the accuracy of a CODAR site.

The pattern measurements shown here indicate that the length of the monopole ground plane and the local environment play an important role in antenna pattern distortion. If the ground plane is resonant or there is interference within the antennas near-field, the ideal geometry of the antenna breaks down and the elements interact. This breakdown has also been shown theoretically to cause inter-element interaction that distorts the antenna pattern (Burke 1992).

#### *b) ADCP Comparisons*

The MUSIC algorithm can use either the measured or ideal pattern to determine the bearing of a given radial velocity. For the purpose of this study, results obtained with the ideal pattern will be called ideal pattern results and those obtained with the measured pattern will be labeled the measured pattern results. The processing can also utilize an angular interpolation scheme to fill in radial data gaps. Since the measured pattern results usually have more data gaps than the ideal pattern results (Paduan et al. 2001), the interpolation was used exclusively on these data. The ideal, measured and measured-interpolated CODAR results were each independently validated against a moored ADCP. As previously mentioned, the CODAR measurement is the average over the surface meter of the water column and the ADCP is a one meter average at a depth of 2.5 meters. Between October 16, 1999 and January 24, 2000, the CODAR sampling was separated into two regimes. From October 16, 1999 to December 4, 1999, the antennas were setup with the resonant 2.4 m ground plane. From December 6, 1999 to January 24, 2000, the ground plane was shortened to the non-resonant 1.2 m. These tests take

advantage of the amplified distortion observed with the resonant ground plane so that the effect of this distortion on system accuracy is more easily observed. Additionally, the ADCP was moored near the edge of the antenna pattern for each remote site, so these comparisons also focus on the portion of the pattern most affected by antenna element interaction. Results from the clear site indicate the influence of the pattern distortion on the ADCP comparisons (Table 2). When the larger ground plane was tested, the ideal pattern results had a RMS difference of 9.53 cm/s and a correlation of 71%. When the large distortion was accounted for in MUSIC by using the measured pattern, the RMS difference improved to 7.37 cm/s with a correlation of 90%. With the non-resonant ground plane, the distortion is significantly reduced and there is only a small difference between the ideal and measured pattern results. The ADCP comparisons show that either pattern has RMS differences on the order of 8 cm/s with an average correlation of 82%. With the near ideal pattern, the accuracy of the CODAR measurement is independent of the pattern used in the processing. However, if these patterns are distorted, surface current measurements are in better agreement when MUSIC uses the measured pattern.

Table 2 also shows the number of concurrent data points from each instrument used in the comparison. One consequence of using the measured pattern in the MUSIC processing is that certain radial directions are favored over others. The number of points used in each comparison indicates this asymmetry in the radial fields. The angular interpolation within a given range cell was used in the processing to fill in these gaps. The interpolated data was compared to the ADCP to assess the validity of the algorithm. With a RMS difference of 7.75 cm/s and a correlation of 86%, the measured-interpolated data correlation is on the same order as the measured pattern data without interpolation. These results hold true for both the resonant and non-resonant cases. With both ground planes, the measured-interpolated data had similar

statistical comparisons as the corrected data and proves to be an effective algorithm for filling in radial data gaps.

The same study was repeated in the cluttered environment. This site differs from the clear site in that the patterns are distorted with both the resonant and non-resonant ground planes. The only similarity is that the distortion near the endpoints was reduced with the shorter ground plane. With the resonant ground plane, the results using the measured pattern improved the ADCP correlation from 84% to 94% (Table 3). These results are consistent with those found at the clear site. With the non-resonant ground plane, the results did not differ significantly between the measured and ideal pattern data. Even with the distortion near the center of the pattern, the reduced distortion near the endpoints is sufficient to equalize the two results. These observations suggest that the distortion near the center of the pattern may not influence the radial data distribution near the edge of the pattern.

Since MUSIC uses the antenna pattern to determine the bearing of each radial velocity observed in a given range cell, comparisons between the ADCP and radial currents from all other angles in the CODAR range cell may indicate why pattern measurements improve system accuracy. The RMS difference between the ADCP and all CODAR grid points was determined for the ideal, measured, and measured-interpolated CODAR data. Since bearing solutions estimated with the ideal pattern are found over 360 degrees and solutions with the measured pattern only occur over the range covered by the boat measurement, solutions over land sometimes are included in the ideal data. Paduan et al. (2001) suggest that the ideal solutions outside the measured pattern domain result from pattern distortion. The angular dependence of the RMS difference between the ADCP and the CODAR data estimated with the ideal pattern has a very broad minimum shifted to the right of the ADCP (Figure 6a). When the data is

processed with the measured pattern, the RMS value at the ADCP is lower and the narrower minimum is shifted toward the ADCP. With the non-resonant ground plane, the angular dependence of the RMS comparison does not differ significantly for the two patterns (Figure 6b). This is to be expected since the two patterns are almost identical and the CODAR estimates should be similar. If the patterns are distorted, the correlation statistics are improved by more consistently placing radial velocities in the appropriate angular bin.

The angular validation at the cluttered site supports the results found in the clear site. If the pattern is distorted, the lowest RMS difference is closer to the ADCP when the measured pattern is used (Figure 6c). Even with the pattern distortion seen with the non-resonant ground plane, the ADCP correlation statistics did not change (Table 3). Similarly, the angular dependence of the RMS difference does not change between the ideal and measured pattern estimates (Figure 6d). With the ADCP location near the edge of the pattern, these results indicate that pattern distortion may only affect local bearing estimates.

The measured and interpolated data for the entire clear site range cell was also compared to the ADCP. If the interpolation is used, the data gaps or spokes seen in the estimates processed with the measured pattern are filled in (Figure 7). The RMS curves for the measured pattern and measured-interpolated pattern data are nearly identical, indicating that the two datasets compare similarly to the ADCP. Since the algorithm is using a twenty-degree window for interpolation and smoothing, the RMS minimum in the interpolated data is broader than the measured result without interpolation (Figure 7). The algorithm used here is an effective method for filling in radial data gaps in the measured pattern data.

The comparisons with the ADCP show that the CODAR data processed with the measured antenna pattern has a higher correlation. These results are especially evident if the

patterns are significantly distorted, as is the case with the resonant ground plane. If the measured and ideal patterns do not significantly differ, the correlation remains high regardless of the pattern used in the processing. This study takes advantage of the ADCPs proximity to the endpoint of the pattern, the area most affected by antenna element interaction. The next section will expand these results over all angles by looking at comparisons between CODAR data processed with the measured and ideal antenna pattern.

*c) Measured vs. Ideal*

The results of the previous section showed that for the angles looking toward the ADCP, system accuracy improved with the measured pattern if significant distortion exists. To spatially extend the ADCP results, this section discusses comparisons between CODAR currents generated with the ideal and the measured antenna patterns over all angles. In the following analysis, data from the clear site CODAR range cell passing through the ADCP was used. Measured pattern currents from a specific angular bin were compared to the ideal pattern currents from all angular bins. The RMS difference calculations were then repeated for each angular bin in the range cell. Figure 8 shows contour plots of the RMS difference between the measured and ideal pattern results. The x-axis is the reference angle from true north for each angular bin of the measured pattern. The y-axis is the relative angle between the measured angular bin and the ideal angular bin. Zero relative angle means the measured and ideal angular bins are collocated, and positive relative angles imply that the ideal angular bin is north of the measured angular bin. The dashed line indicates the ideal bin with the lowest RMS difference. Since the reference angle in each plot does not match the relative angle near the edges, the measured pattern focuses the possible angle solutions to a narrower range and the ideal pattern

spreads the possible solutions over more angles. When the patterns are distorted, the measured and ideal pattern data measured at the same angular bin do not have the lowest RMS difference (Figure 8a). The dashed line shows that the lowest RMS difference could be with a grid point as far as 50 degrees away. This angular offset is shown to be dependent on the reference angle, with a larger offset near the edges. This appears to be related to the increased distortion observed near the coast. If the resonant ground plane is replaced with a shorter non-resonant ground plane, the distortion near the edge of the pattern is reduced. The ideal bin with the best correlation to the measured pattern result is much closer to the measured pattern data point (Figure 8b). This is to be expected since the measured pattern is almost ideal.

## **5. Conclusion**

As the role of HF radar becomes increasingly more important in coastal observatories and regional modeling efforts, it is imperative to properly maintain accurate systems to ensure high data quality. System accuracy is shown to be dependent on the distortion of the measured pattern. For the CODAR-type DF system, this distortion is related to the interaction between the individual elements, whether caused by a resonant ground plane or the local environment. In many cases distortion is unavoidable due to site location constraints. For these instances it is necessary to process the data with the measured pattern. Unless the measured pattern is nearly ideal, ADCP comparisons indicate that the CODAR bearing estimates are more accurate if MUSIC uses the measured pattern. A direct CODAR to CODAR comparison shows that the offset between the measured and ideal angular bins with the lowest RMS difference extends over all angles when the pattern is distorted over all angular bins. To maximize a HF radar's usefulness for scientific and operational applications, the antenna patterns for each site must be

measured and, if distorted, these patterns should be used in the processing to improve the surface current measurements.

***Acknowledgements.*** This work was funded by the Office of Naval Research (N00014-97-1-0797, N00014-99-1-0196, N00014-00-1-0724), the National Ocean Partnership Program (N00014-97-1-1019, N000-14-98-1-0815), and the great state of New Jersey. ADCP data provided by the Mid-Atlantic Bight National Undersea Research Center with additional support from the National Science Foundation.

## References

- Barrick, D.E., 1972: First-order theory and analysis of mf/hf/vhf scatter from the sea. *IEEE Trans. Antennas Propag*, AP-20, 2-10.
- Barrick, D.E., M.W. Evens and B.L. Weber, 1977: Ocean surface currents mapped by radar. *Science*, 198, 138-144.
- Barrick, D.E. and B.J. Lipa, 1986: Correcting for distorted antenna patterns in CODAR ocean surface measurements. *IEEE J. Ocean. Eng*, OE-11, 304-309.
- Barrick, D.E. and B.J. Lipa, 1996: Comparison of direction-finding and beam-forming in hf radar ocean surface current mapping. Phase 1 SBIR final report. Contract No. 50-DKNA-5-00092. National Oceanic and Atmospheric Administration, Rockville, MD.
- Barrick, D.E. and B.J. Lipa, 1997: Evolution of bearing determination in hf current mapping radars. *Oceanography*, 10, 72-75.
- Barrick, D.E. and B.J. Lipa, 1999: Radar angle determination with MUSIC direction finding. United States Patent, No. 5,990,834.
- Breivik, O. and O. Sætra, 2001: Real time assimilation of hf radar currents into a coastal ocean model. *J. Marine Systems*, 28, 161-182.
- Burke, G. J. , 1992: Numerical Electromagnetics Code -- NEC-4, UCRL-MA-109338, Parts I & II, Lawrence Livermore National Laboratory, Livermore, CA.
- Chapman, R.D. and H.C. Graber, 1997: Validation of hf radar measurements. *Oceanography*, 10, 76-79.
- Chapman, R.D., L.K. Shay, H.C. Graber, J.B. Edson, A. Karachintsev, C.L. Trump and D.B. Ross, 1997: On the accuracy of hf radar surface current measurements: intercomparisons with ship-based sensors. *J. Geophys. Res*, 102, 18,737-18,748.
- Crombie, D.D., 1955: Doppler spectrum of sea echo at 13.56 Mc/s. *Nature*, 175, 681-682.
- Fernandez, D.M., H.C. Graber, J.D. Paduan and D. E. Barrick, 1997: Mapping wind direction with hf radar. *Oceanography*, 10, 93-95.
- Fernandez, D.M. and J.D. Paduan, 1996: Simultaneous CODAR and OSCAR measurements of ocean surface currents in Monterey Bay. Proceedings, IEEE IGARSS '96, Lincoln, Neb, 3, 1746-1750.
- Furukawa, K. and M.L. Heron, 1996: Vortex modeling and observation of a tidally induced jet.

- Coastal Engineering*, Japan Society of Civil Engineering, 43, 371-375.
- Glenn, S.M., W. Boicourt, B. Parker and T.D. Dickey, 2000: Operational observation networks for ports, a large estuary and an open shelf. *Oceanography*, 13, 12-23.
- Glenn, S.M., T.D. Dickey, B. Parker and W. Boicourt, 2000: Long-term real-time coastal ocean observation networks. *Oceanography*, 13, 24-34.
- Graber, H.C., B.K. Haus, L.K. Shay and R.D. Chapman, 1997: Hf radar comparisons with moored estimates of current speed and direction: expected differences and implications. *J. Geophys. Res.*, 102, 18,749-18,766.
- Graber, H.C. and M.L. Heron, 1997: Wave height measurements from hf radar. *Oceanography*, 10, 90-92.ICON;
- Grassle, J.F., S.M. Glenn and C. von Alt, 1998: Ocean observing systems for marine habitats. *OCC '98 Proceedings*, Marine Technology Society, November, 567-570.
- Kohut, J.T., 2002: Spatial Current Structure Observed With a Calibrated HF Radar System: The Influence of Local Forcing, Stratification, and Topography on the Inner Shelf. Ph.D. Thesis. Rutgers University. 141 pgs.
- Kohut, J. T., S. M. Glenn and D. E. Barrick, 1999: SeaSonde is Integral to Coastal Flow Model Development. *Hydro International*, 3, 32-35.
- Kohut, J.T., S.M. Glenn and D.E. Barrick, 2000: Multiple hf-radar system development for a regional longterm ecosystem observatory in the New York bight. *American Meteorological Society: Fifth Symposium on Integrated Observing Systems*, 4-7.
- Kosro, P.M., J.A. Barth and P.T. Strub, 1997: The coastal jet: observations of surface currents over the Oregon continental shelf from hf radar. *Oceanography*, 10, 53-56.
- Laws, K., D.M. Fernandez and J.D. Paduan, 2001: Simulation-based evaluations of hf radar ocean current algorithms. *J. Oceanic Engin*, 25, 481-491.
- Lipa, B.J. and D.E. Barrick. 1983: Least-squares methods for the extraction of surface currents from CODAR cross-loop data: application at ARSLOE. *IEEE J. Ocean. Engr*, OE-8, 226-253.
- Lipa, B.J. and D.E. Barrick, 1986: Extraction of sea state from hf-radar sea echo: mathematical theory and modeling. *Radio Sci*, 21, 81-100.
- Oke , P.R., J.S. Allen, R.N. Miller, G.D. Egbert and P.M. Kosro, 2000: Assimilation of surface velocity data into a primitive equation coastal ocean model. *J. Geophys. Res.* submitted.
- Paduan, J.D., D.E. Barrick, D.M. Fernandez, Z. Hallok and C.C. Teague, 2001: Improving the

- accuracy of coastal hf radar current mapping. *Hydro International*, 5, 26-29.
- Paduan, J.D., L.K. Rosenfeld, S.R. Ramp, F. Chavez, C.S. Chiu and C.A. Collins, 1999: Development and maintenance of the ICON observing system in Monterey Bay. Proceedings, American Meteorological Society's Third Conference on Coastal Atmospheric and Oceanic Prediction and Processes, New Orleans, LA, 3-5 November, 226-231.
- Paduan, J.D., D.E. Barrick, D.M. Fernandez, Z. Hallok and C.C. Teague, 2001: Improving the accuracy of coastal hf radar current mapping. *Hydro International*, 5, 26-29.
- Paduan, J.D. and M.S. Cook, 1997: Mapping surface currents in Monterey Bay with CODAR-type hf radar. *Oceanography*, 10, 49-52.
- Paduan, J.D. and H.C. Graber, 1997: Introduction to high-frequency radar: reality and myth. *Oceanography*, 10, 36-39.
- Schmidt, R.O., 1986: Multiple emitter location and signal parameter estimation. *IEEE Trans. Antennas Propag*, AP-34, 276-280.
- Schofield, O., T. Bergmann, W.P. Bissett, F. Grassle, D Haidvogel, J. Kohut, M. Moline and S. Glenn, 2001: The long term ecosystem observatory: an integrated coastal observatory. *IEEE J. Ocean. Engin.*, In press.
- Shay, L.K., H.C. Graber, D.B. Ross and R.D. Chapman, 1995: Mesoscale ocean surface current structure detected by hf radar. *J. Atmos. Ocean. Tech*, 12, 881-900.
- Shulman, I., C.R. Wu, J.K. Lewis, J.D. Paduan, L.K. Rosenfeld, S.R. Ramp, M.S. Cook, J.D. Kindle and D.S. Ko, 2000: Development of the high resolution, data assimilation numerical model of the Monterey Bay. In *Estuarine and Coastal Modeling*, Spaulding, M.L. and H. Lee Butler, eds., 980-994.
- Stewart, R.H. and J.W. Joy, 1974: Hf radio measurement of surface currents. *Deep-Sea Res.*, 21, 1039-1049.
- Teague, C.C., J.F. Vesecky and D.M. Fernandez, 1997: Hf radar instruments, past to present. *Oceanography*, 10, 40-44.
- Wyatt, L.R., 1997: The ocean wave directional spectrum. *Oceanography*, 10, 85-89.

Figure 1. Study area off the southern coast of New Jersey including hourly radial maps from the Brant Beach (red) and Brigantine (blue) sites. The solid semicircle highlights a range cell for the Brant Beach Site.

Figure 2. Ideal (thin dashed) and measured antenna patterns for loop 1 (thick solid) and loop 2 (thick dash-dot) normalized by the monopole. The measured pattern data was collected during run 2.

Figure 3. Normalized antenna pattern distortion for loop 1 (solid) and loop 2 (dash-dot) measured at the clear Brant Beach site for (a) run 3, (b) run 4, (c) run 6 and (d) run 7.

Figure 4. Normalized antenna pattern distortion for loop 1 (solid) and loop 2 (dash-dot) measured at the cluttered Brigantine site for (a) run 1, (b) run 2, (c) run 12, (d) run 10 and (e) run 13.

Figure 5. Antenna patterns of loop 1 (thick solid) and loop 2 (thick dash-dot) normalized by the monopole at the clear site during (a) run 5 and (b) run 8.

Figure 6. RMS difference between the radial velocities of the ADCP and each CODAR angular bin within the range cell passing through the ADCP using the measured (solid) and ideal (dashed) antenna patterns. Comparisons were made at the clear site with the (a) resonant and (b) non-resonant ground plane, and repeated at the cluttered site with both the (c) resonant and (d) non-resonant ground plane. The angular bin containing the ADCP is shown as a vertical black line.

Figure 7. RMS difference (upper lines) at the clear site between the radial velocities of the ADCP and each CODAR angular bin within the range cell passing through the ADCP using the measured antenna pattern with (dashed) and without (solid) the interpolation-smoothing algorithm. The number of data points (lower lines) for each angular bin with (dashed) and without (solid) the interpolation-smoothing algorithm.

Figure 8. RMS difference between the measured and ideal pattern current estimates at the clear site with the (a) resonant and (b) non-resonant ground planes. The lowest RMS difference for each bin is shown as a dashed line.

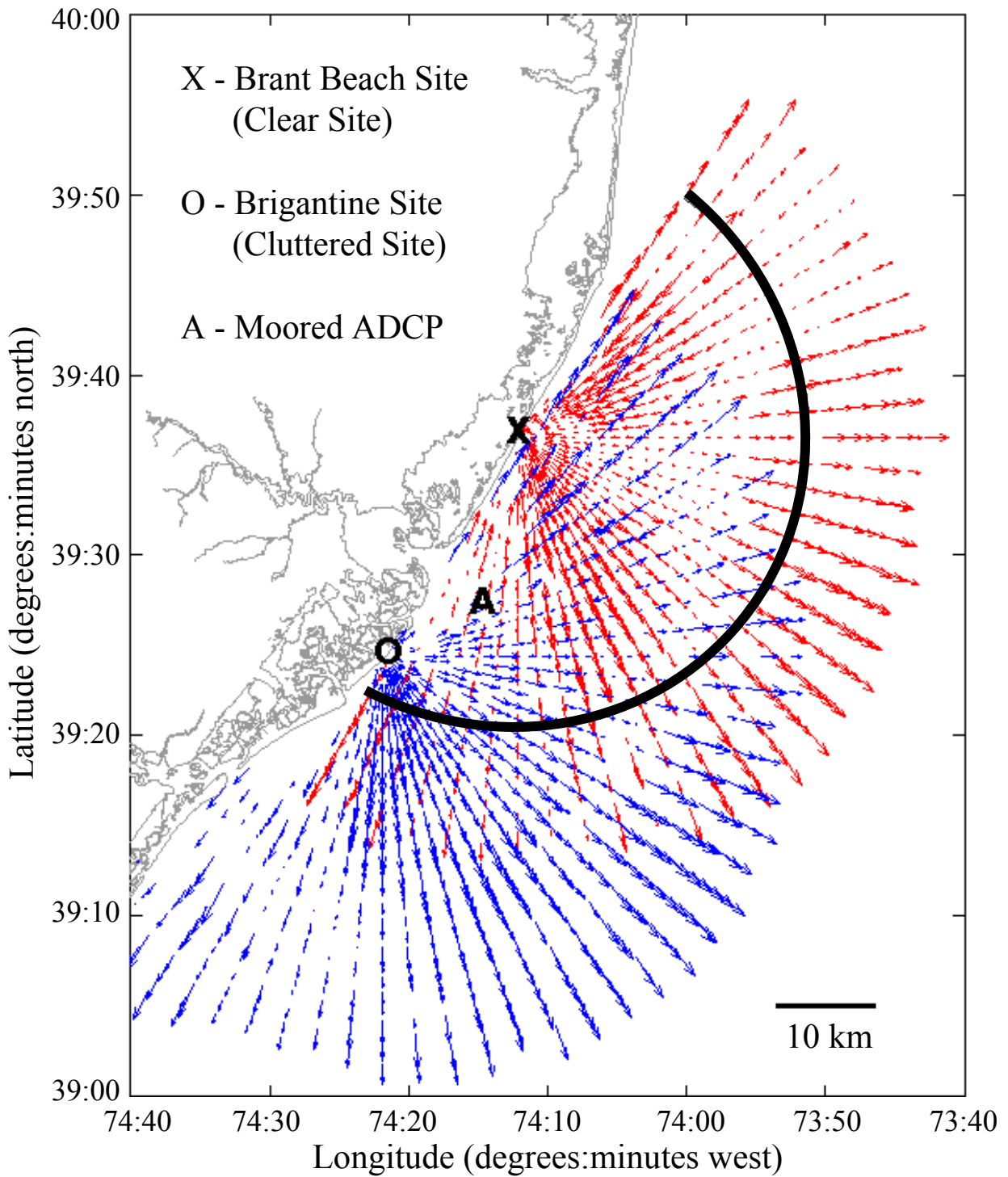


Figure 1. Study area off the southern coast of New Jersey including hourly radial maps from the Brant Beach (red) and Brigantine (blue) sites. The solid semicircle highlights a range cell for the Brant Beach Site.

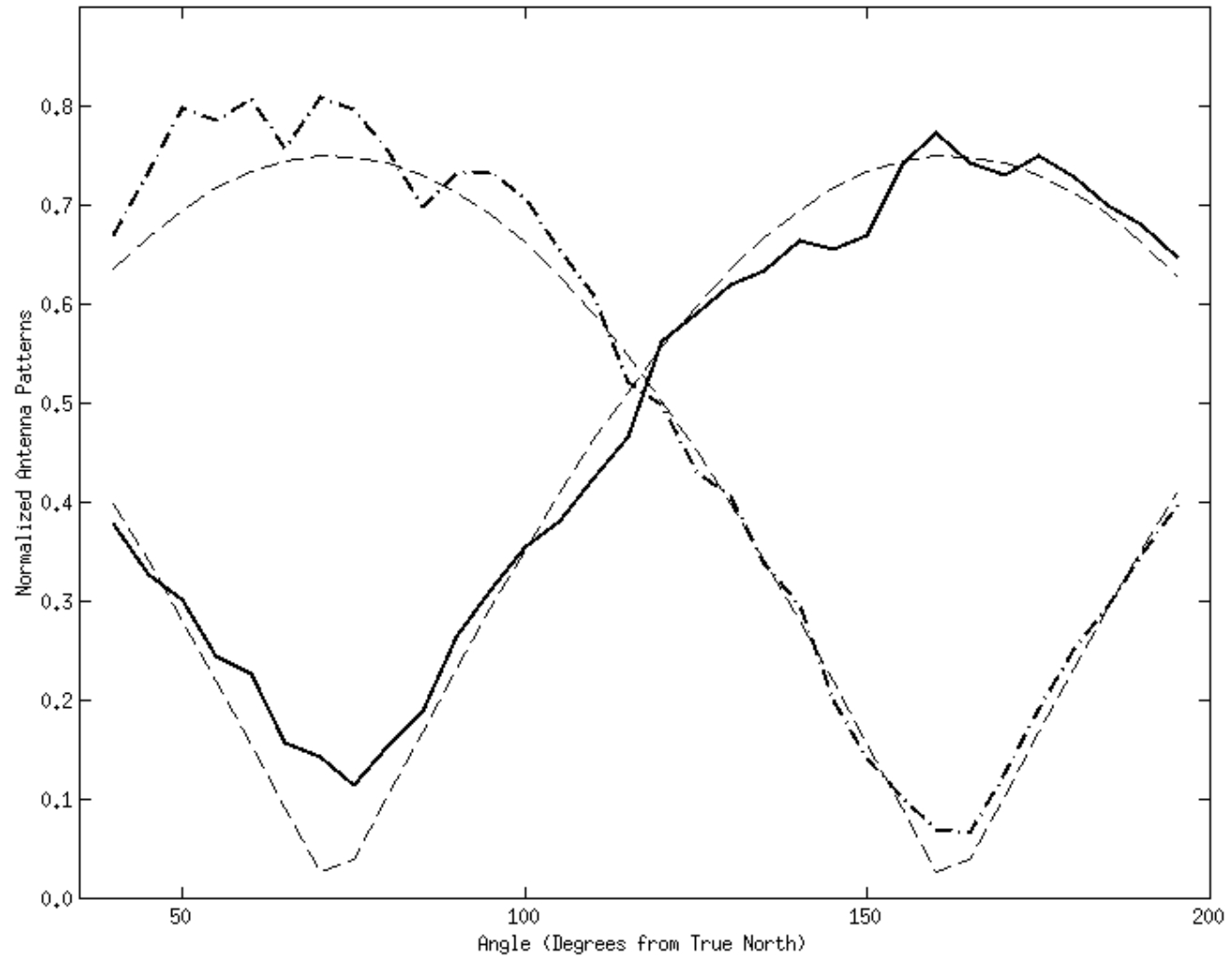


Figure.2 Ideal (thin dashed) and measured antenna patterns for loop 1 (thick solid) and loop 2 (thick dash-dot) normalized by the monopole.

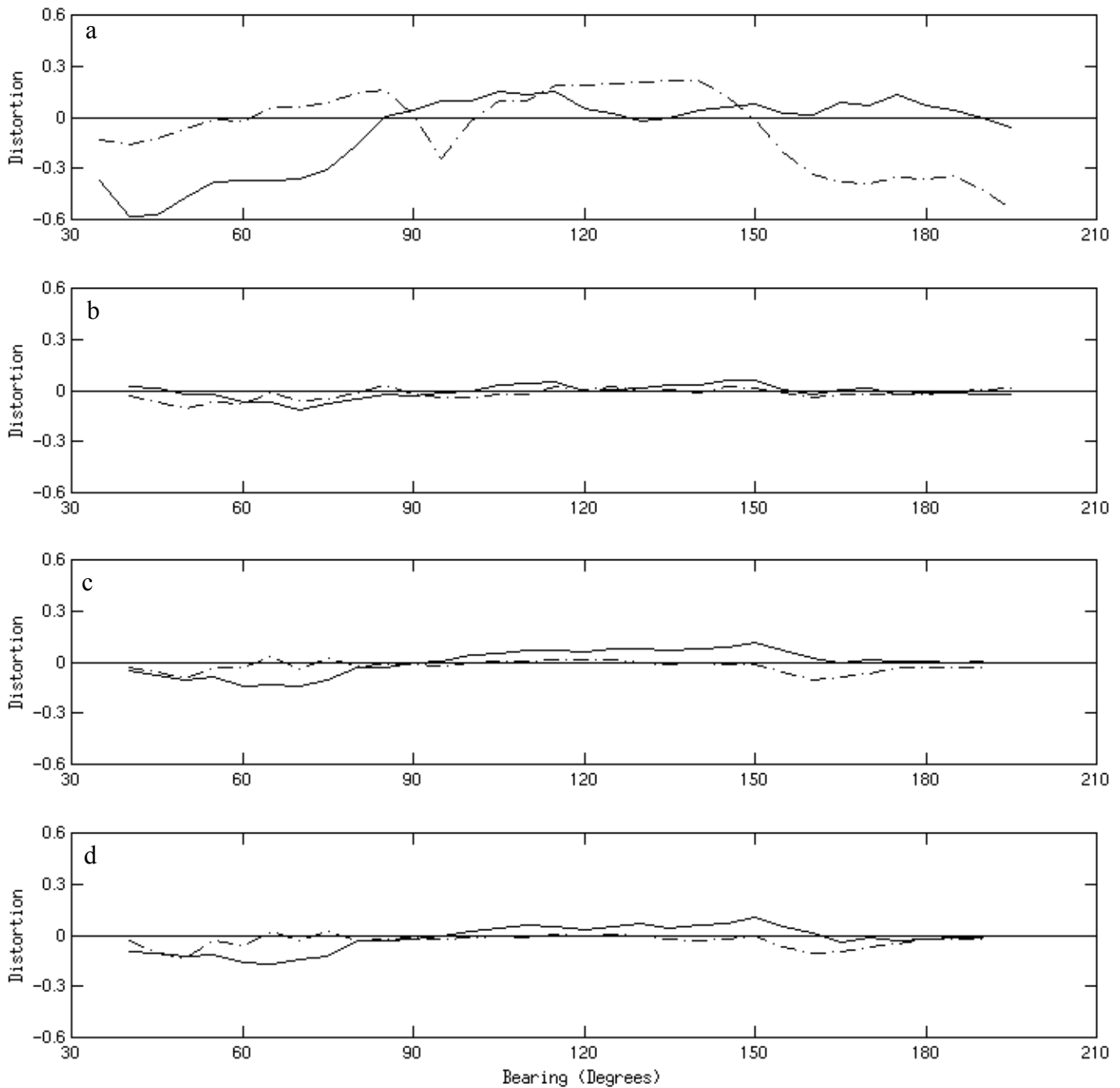


Figure 3. Normalized antenna pattern distortion for loop 1 (solid) and loop 2 (dash-dot) measured at the clear Brant Beach site for (a) run 3, (b) run 4, (c) run 6 and (d) run 7.

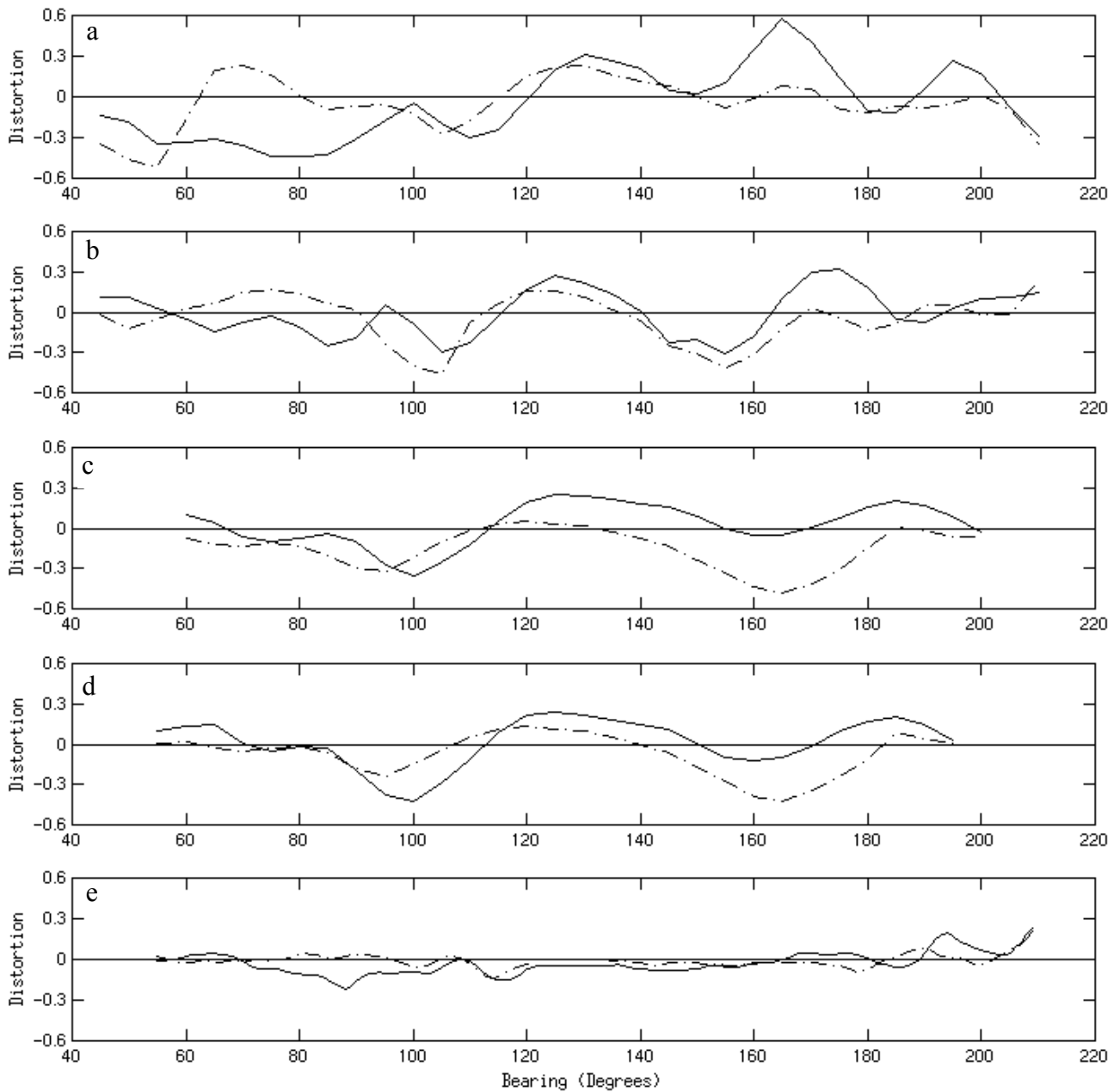


Figure.4. Normalized antenna pattern distortion for loop 1(solid) and loop2 (dash-dot) measured at the cluttered Brigantine site for (a) run 1, (b) run 2, (c) run 12, (d) run 10 and (e) run 13.

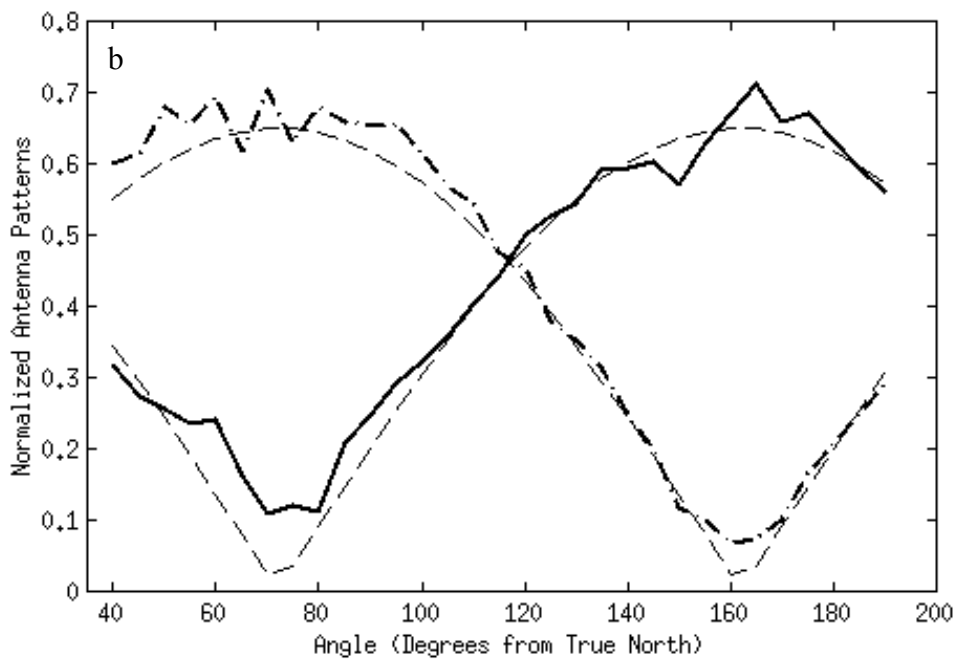
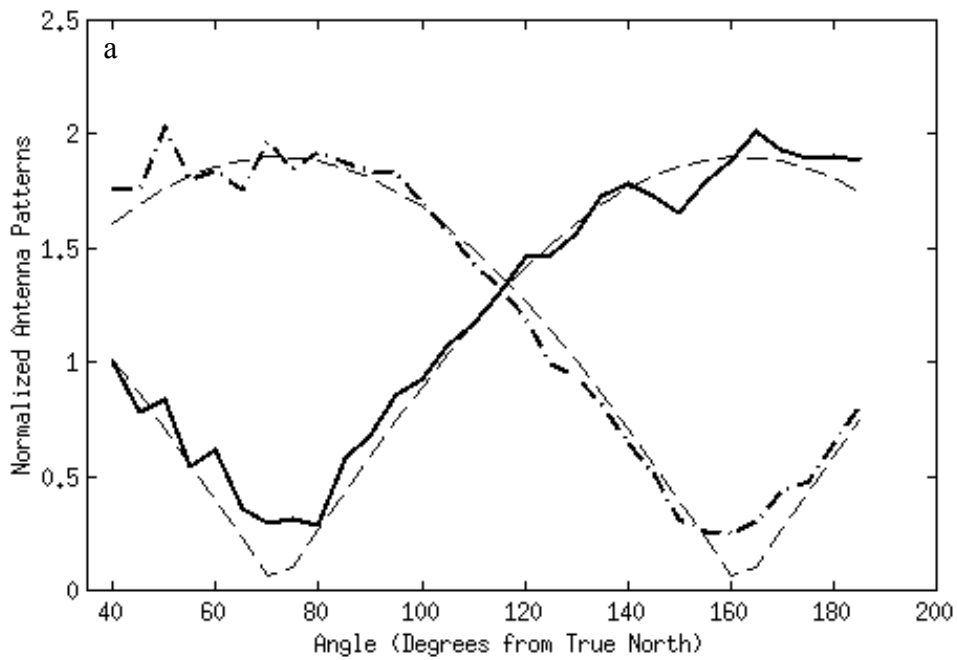


Figure 5. Antenna patterns of loop 1 (thick solid) and loop 2 (thick dash-dot) normalized by the monopole in the clear site during (a) run 5 and (b) run 8.

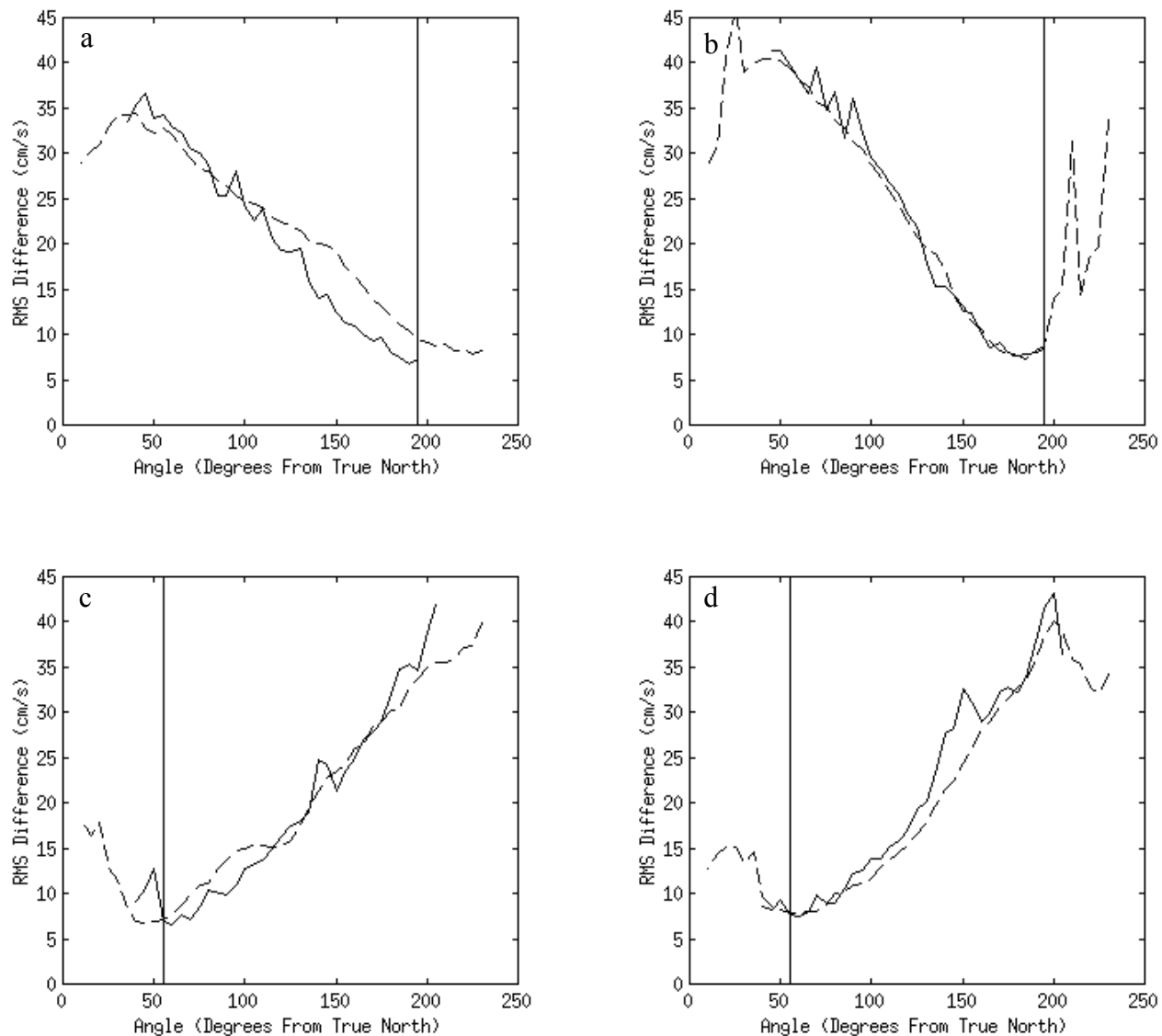


Figure 6. RMS difference between the radial velocities of the ADCP and each CODAR angular bin within the range cell passing through the ADCP using the measured (solid) and ideal (dashed) antenna patterns. Comparisons were made at the clear site with the (a) resonant and (b) non-resonant ground plane, and repeated at the cluttered site with both the (c) resonant and (d) non-resonant ground plane. The angular bin containing the ADCP is shown as a vertical black line.

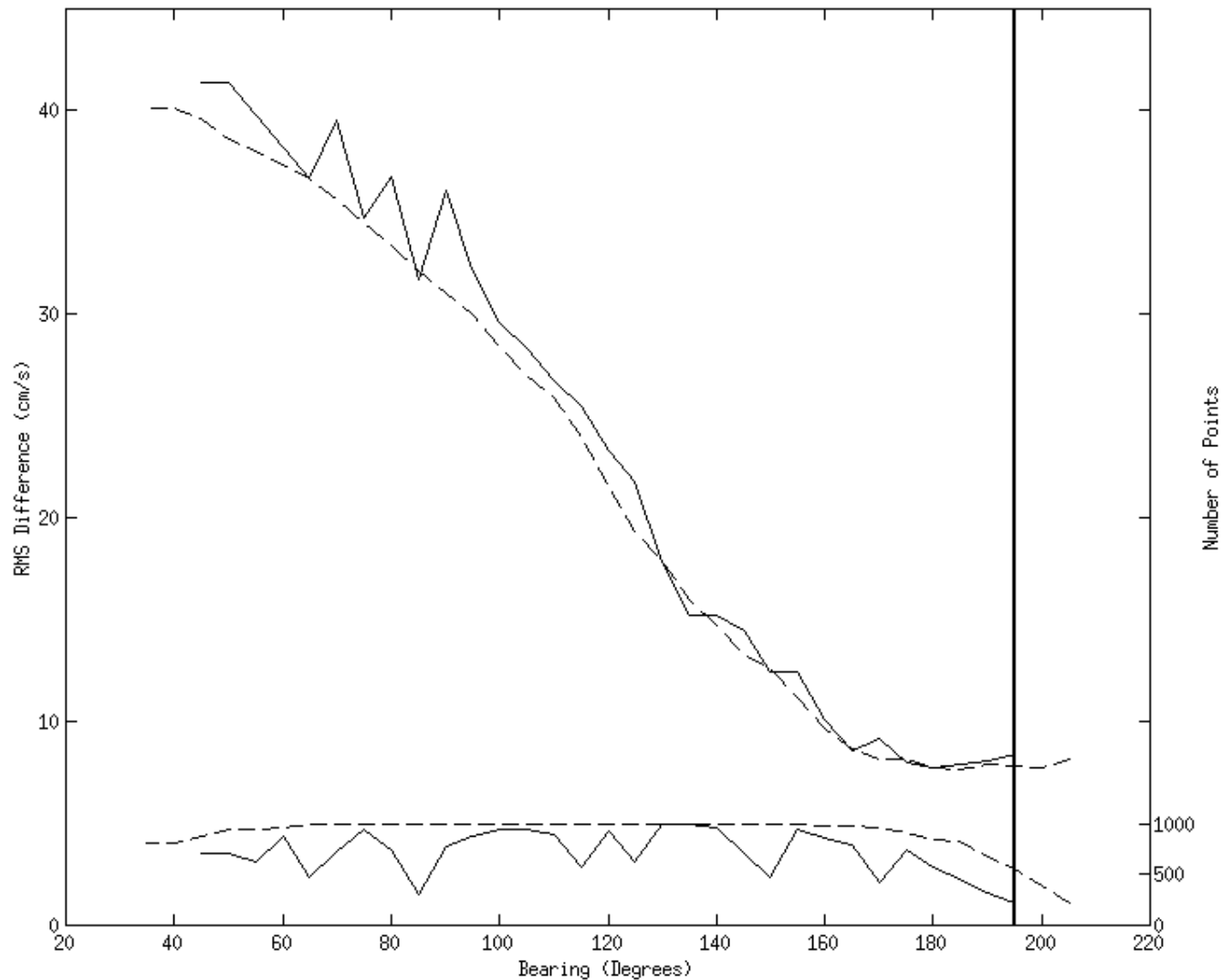


Figure 7. RMS difference (upper lines) at the clear site between the radial velocities of the ADCP and each CODAR angular bin within the range cell passing through the ADCP using the measured antenna pattern with (dashed) and without (solid) the interpolation-smoothing algorithm. The number of data points (lower lines) for each angular bin with (dashed) and without (solid) the interpolation-smoothing algorithm.

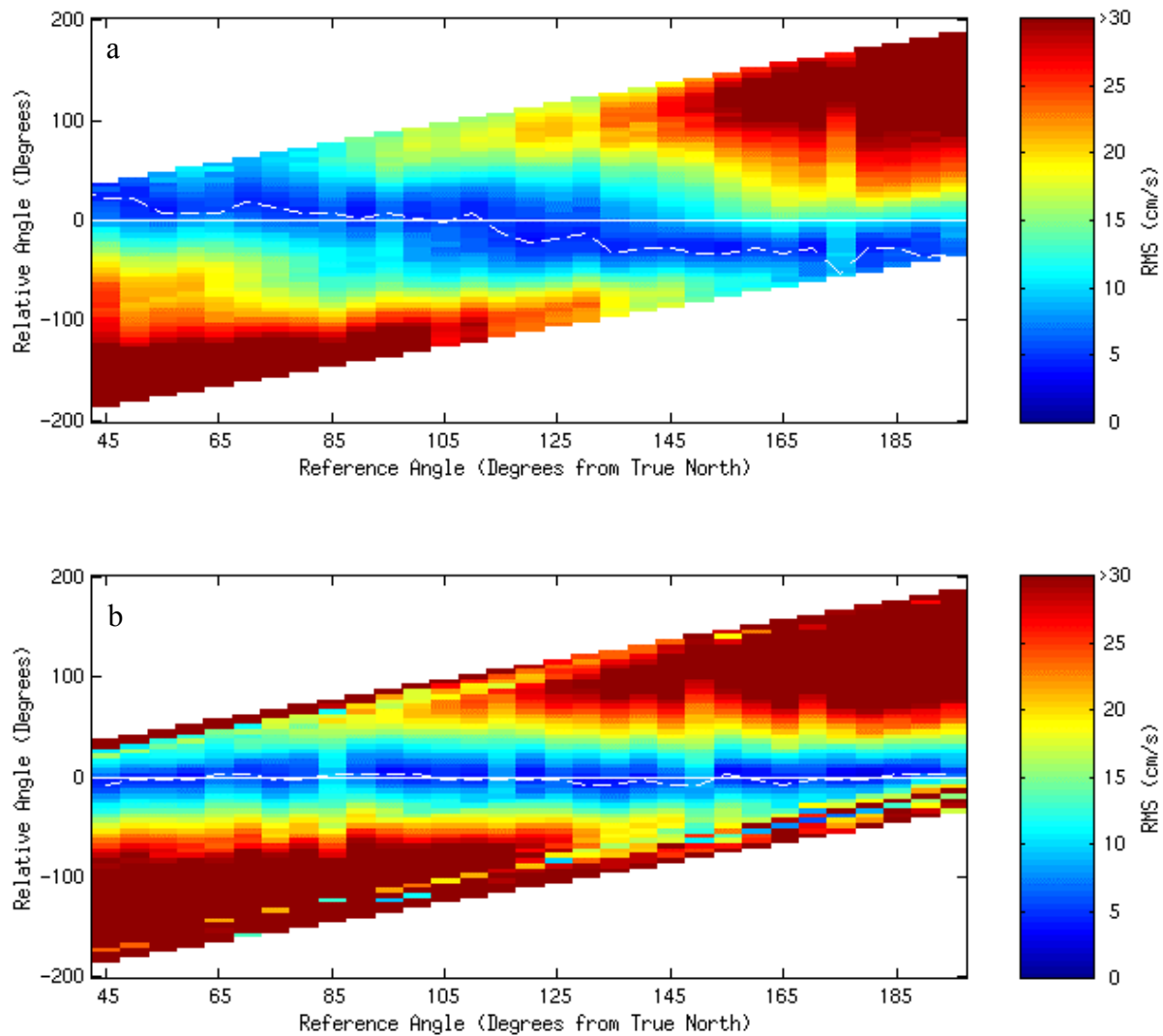


Figure 8. RMS difference between the measured and ideal pattern current estimates at the clear site with the (a) resonant and (b) non-resonant ground planes. The lowest RMS difference for each bin is shown as a dashed line.

Table 2.1. Antenna Pattern Measurement Runs					
Run Number	Ground Plane	Environment	Antenna	Receiver	Date
1	2.4 m	Cluttered	B	B	October, 1999
2	1.2 m	Cluttered	B	B	October, 1999
3	2.4 m	Clear	A	A	October, 1999
4	1.2 m	Clear	A	A	October, 1999
5	1.2 m	Clear	A	A	September, 2000
6	1.2 m	Clear	B	A	September, 2000
7	1.2 m	Clear	B	B	September, 2000
8	1.2 m	Clear	A	A	September, 2000
9	1.2 m	Cluttered	B	B	November, 2000
10	1.2 m	Cluttered	A	B	November, 2000
11	1.2 m	Cluttered	B	B	November, 2000
12*	1.2 m	Cluttered	B	B	November, 2000
13	1.2 m	Cluttered (New)	B	B	October, 2001

\* Same as run 11 except different cable location.

Table 2.2 ADCP Comparison Statistics for the Clear Environment				
Ground Plane	Antenna Pattern	RMS Difference	R <sup>2</sup>	Number of Points
2.4 m	Ideal	9.53 cm/s	71%	682
2.4 m	Measured	7.37 cm/s	90%	314
2.4 m	Measured-Interpolated	7.75 cm/s	86%	594
1.2 m	Ideal	8.30 cm/s	81%	99
1.2 m	Measured	8.40 cm/s	83%	224
1.2 m	Measured-Interpolated	7.80 cm/s	88%	549

Table 2.3. ADCP Comparison Statistics for the Cluttered Environment				
Ground Plane	Antenna Pattern	RMS Difference	R <sup>2</sup>	Number of Points
2.4 m	Ideal	7.19 cm/s	84%	699
2.4 m	Measured	6.83 cm/s	94%	190
2.4 m	Measured-Interpolated	7.65 cm/s	82%	722
1.2 m	Ideal	7.76 cm/s	90%	694
1.2 m	Measured	7.68 cm/s	93%	632
1.2 m	Measured-Interpolated	6.70 cm/s	90%	920